Proceedings of the XII Finnish Mechanics Days
R. Kouhia, J. Mäkinen, S. Pajunen and T. Saksala (Eds.)

On the effect of damping on stability of non-conservative systems

Juha Jeronen[1 2] and Reijo Kouhia[2]

[(1)]University of Jyväskylä, Department of Mathematical Information Technology
P.O. Box 35, 40014 University of Jyväskylä, Finland, juha.jeronen@jyu.fi
[(2)]Tampere University of Technology, Department of Mechanical Engng and Industrial Systems
P.O. Box 589, 33101 Tampere, Finland, reijo.kouhia@tut.fi

Summary. Anomalous damping-induced destabilization is investigated in a simple, small system consisting of a double pendulum with springs. Linearized and fully non-linear results are presented.

Key words: stability, follower force, damping, two-dof model, destabilization paradox

Introduction

In 1952 Hans Ziegler reported an anomaly observed in the stability analysis of a simple double pendulum model consisting of linear springs and dampers, and loaded by a follower force at the free end [1]. Addition of small dissipative forces in the system resulted in an destabilizing effect, which is a counterintuitive result and is often called a paradox. For a system in equilibrium under the action of potential forces, the addition of dissipative forces with complete dissipation ensures asymptotic stability of the undisturbed equilibrium, as stated by the well known Kelvin's theorem [2, Page 75]. However, such a result does not exist for general non-conservative systems.

Even though the problem is more than 60 years old, and numerous investigations have been carried out on the understanding of the eigenvalue behaviour near the discontinuity at zero damping, it is not fully understood. Bolotin attributes the controversial result to the inability of the linear approximation to assess the question of stability [2, Pages 99-100], [3]. An attempt to a physical explanation is given in a rather recent paper by Sugiyama and Langthjem [4].

In this paper, behaviour of the Ziegler's pendulum with vanishing dissipation is reinvestigated by using the fully non-linear model.

Two degree-of-freedom model

A double pendulum subjected to a follower force is studied, see Fig. 1. The bars are connected to each other, and to a fixed support with an elastic spring and a linear viscous damper. In the seminal paper [1], Ziegler found that the critical load in the case of small damping can be smaller than the critical load without damping. This result, a jump in the critical load at vanishinly small damping is often called *the paradox of destabilization due to damping.*

To obtain the equations of motion, the principle of virtual work is applied:

$$\delta W_i + \delta W_e + \delta W_j = 0 \,, \tag{1}$$

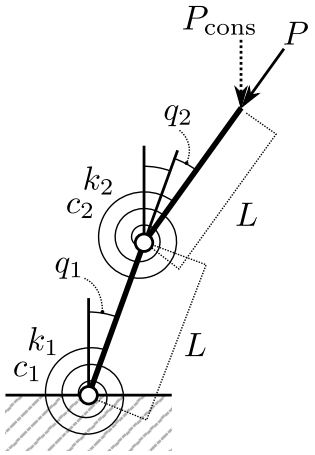

Figure 1. Problem setup.

where the internal, external and inertial parts of the virtual work have the expressions

$$\delta W_i = -\left(k_1 q_1 + c_1 \dot{q}_1\right)\delta q_1 - \left(k_2 q_2 + c_2 \dot{q}_2\right)\delta q_2 \,, \tag{2}$$

$$\delta W_e = -PL\sin(q_2)\delta q_1 \,, \tag{3}$$

$$\begin{aligned}\delta W_j = &-mL^3\left[\left(\tfrac{5}{3}+\cos(q_2)\right)\ddot{q}_1 + \left(\tfrac{1}{3}+\tfrac{1}{2}\cos(q_2)\right)\ddot{q}_2 - \sin(q_2)\dot{q}_1\dot{q}_2 - \tfrac{1}{2}\sin(q_2)(\dot{q}_2)^2\right]\delta q_1 \\ &-mL^3\left[\left(\tfrac{1}{3}+\tfrac{1}{2}\cos(q_2)\right)\ddot{q}_1 + \tfrac{1}{3}\ddot{q}_2 + \tfrac{1}{2}\sin(q_2)(\dot{q}_1)^2\right]\delta q_2 \,,\end{aligned} \tag{4}$$

where k_1, k_2 are the spring stiffnesses, c_1, c_2 the damping coefficients, L the length of one rod and P the magnitude of the follower force $\mathbf{P}$. The virtual work equation (1) can be written, as used in Ref. [6], in the form

$$(\mathbf{L} + \mathbf{Q} + \mathbf{J}) \cdot \delta\mathbf{q} = 0 \,, \tag{5}$$

where the internal, external and inertial generalized forces are

$$\begin{aligned}\mathbf{L} &= -\begin{bmatrix} k_1 q_1 + c_1 \dot{q}_1 \\ k_2 q_2 + c_2 \dot{q}_2 \end{bmatrix}, \qquad \mathbf{Q} = -PL\begin{bmatrix} \sin q_2 \\ 0 \end{bmatrix}, \\ \mathbf{J} &= -mL^3\begin{bmatrix} \left(\tfrac{5}{3}+\cos(q_2)\right)\ddot{q}_1 + \left(\tfrac{1}{3}+\tfrac{1}{2}\cos(q_2)\right)\ddot{q}_2 - \sin(q_2)\dot{q}_1\dot{q}_2 - \tfrac{1}{2}\sin(q_2)(\dot{q}_2)^2 \\ \left(\tfrac{1}{3}+\tfrac{1}{2}\cos(q_2)\right)\ddot{q}_1 + \tfrac{1}{3}\ddot{q}_2 + \tfrac{1}{2}\sin(q_2)(\dot{q}_1)^2 \end{bmatrix}.\end{aligned} \tag{6}$$

For comparison, in the conservative dead-weight loading case with $\mathbf{P}_{\text{cons}}$ (refer to Fig. 1), the corresponding external generalized force becomes (note the opposite sign)

$$\mathbf{Q}_{\text{cons}} = P_{\text{cons}} L \begin{bmatrix} \sin q_1 + \sin(q_1+q_2) \\ \sin(q_1+q_2) \end{bmatrix}.$$

Because the variation $\delta\mathbf{q}$ is arbitrary, the virtual work equation (5) results in the equations of motion

$$\mathbf{L} + \mathbf{Q} + \mathbf{J} = \mathbf{0} \,. \tag{7}$$

Equation (7) together with Eqs. (6), and proper initial conditions for $\mathbf{q}$ and $\dot{\mathbf{q}}$, completes the non-linear description for the dynamics of the considered two-rod system.

Linearization

Beside the original non-linear model, it will be useful to consider its linearization at some particular point $(\mathbf{q}_e, \dot{\mathbf{q}}_e, \ddot{\mathbf{q}}_e)$. Let us define the perturbations

$$(\mathbf{q}^*, \dot{\mathbf{q}}^*, \ddot{\mathbf{q}}^*) \equiv (\mathbf{q} - \mathbf{q}_e \,,\; \dot{\mathbf{q}} - \dot{\mathbf{q}}_e \,,\; \ddot{\mathbf{q}} - \ddot{\mathbf{q}}_e) \,, \tag{8}$$

and choose the point of linearization as an arbitrary static equilibrium point $(\mathbf{q}_e, \dot{\mathbf{q}}_e, \ddot{\mathbf{q}}_e) = (\mathbf{q}_e, 0, 0)$. Developing a multivariate Taylor series at $(\mathbf{q}_e, 0, 0)$ up to first order results in the following expressions:

$$\widehat{\mathbf{L}}(\mathbf{q}^*, \dot{\mathbf{q}}^*, \ddot{\mathbf{q}}^*) \equiv \mathbf{L}(\mathbf{q}_e, 0, 0) + \frac{\partial \mathbf{L}}{\partial \mathbf{q}}(\mathbf{q}_e, 0, 0)\, \mathbf{q}^* + \frac{\partial \mathbf{L}}{\partial \dot{\mathbf{q}}}(\mathbf{q}_e, 0, 0)\, \dot{\mathbf{q}}^* + \frac{\partial \mathbf{L}}{\partial \ddot{\mathbf{q}}}(\mathbf{q}_e, 0, 0)\, \ddot{\mathbf{q}}^* \,, \tag{9}$$

$$\widehat{\mathbf{Q}}(\mathbf{q}^*, \dot{\mathbf{q}}^*, \ddot{\mathbf{q}}^*) \equiv \mathbf{Q}(\mathbf{q}_e, 0, 0) + \frac{\partial \mathbf{Q}}{\partial \mathbf{q}}(\mathbf{q}_e, 0, 0)\, \mathbf{q}^* + \frac{\partial \mathbf{Q}}{\partial \dot{\mathbf{q}}}(\mathbf{q}_e, 0, 0)\, \dot{\mathbf{q}}^* + \frac{\partial \mathbf{Q}}{\partial \ddot{\mathbf{q}}}(\mathbf{q}_e, 0, 0)\, \ddot{\mathbf{q}}^* \,, \tag{10}$$

$$\widehat{\mathbf{J}}(\mathbf{q}^*, \dot{\mathbf{q}}^*, \ddot{\mathbf{q}}^*) \equiv \mathbf{J}(\mathbf{q}_e, 0, 0) + \frac{\partial \mathbf{J}}{\partial \mathbf{q}}(\mathbf{q}_e, 0, 0)\, \mathbf{q}^* + \frac{\partial \mathbf{J}}{\partial \dot{\mathbf{q}}}(\mathbf{q}_e, 0, 0)\, \dot{\mathbf{q}}^* + \frac{\partial \mathbf{J}}{\partial \ddot{\mathbf{q}}}(\mathbf{q}_e, 0, 0)\, \ddot{\mathbf{q}}^* \,. \tag{11}$$

The hat denotes a first-order Taylor approximation. The linearized equations of motion (7) at the specific point $(\mathbf{q}_e, 0, 0)$ have the form

$$\frac{\partial \mathbf{J}}{\partial \ddot{\mathbf{q}}}(\mathbf{q}_e, 0, 0)\, \ddot{\mathbf{q}}^* + \frac{\partial \mathbf{L}}{\partial \dot{\mathbf{q}}}(\mathbf{q}_e, 0, 0)\, \dot{\mathbf{q}}^* + \left(\frac{\partial \mathbf{L}}{\partial \mathbf{q}}(\mathbf{q}_e, 0, 0) + \frac{\partial \mathbf{Q}}{\partial \mathbf{q}}(\mathbf{q}_e, 0, 0) \right) \mathbf{q}^* = \mathbf{0} \,, \tag{12}$$

which can be written in matrix form as

$$\mathbf{M}\ddot{\mathbf{q}}^* + \mathbf{C}\dot{\mathbf{q}}^* + \mathbf{K}\mathbf{q}^* = \mathbf{0} \,, \tag{13}$$

where the stiffness, damping and mass matrices are

$$\mathbf{K} \equiv -\left(\frac{\partial \mathbf{L}}{\partial \mathbf{q}}(\mathbf{q}_e, 0, 0) + \frac{\partial \mathbf{Q}}{\partial \mathbf{q}}(\mathbf{q}_e, 0, 0) \right) \,, \quad \mathbf{C} \equiv -\frac{\partial \mathbf{L}}{\partial \dot{\mathbf{q}}}(\mathbf{q}_e, 0, 0) \,, \quad \mathbf{M} \equiv -\frac{\partial \mathbf{J}}{\partial \ddot{\mathbf{q}}}(\mathbf{q}_e, 0, 0) \,. \tag{14}$$

Evaluating the differentiations gives

$$\mathbf{K} = \begin{bmatrix} k_1 & 0 \\ 0 & k_2 \end{bmatrix} + PL \begin{bmatrix} 0 & \cos q_2 \\ 0 & 0 \end{bmatrix} \,, \quad \mathbf{C} = \begin{bmatrix} c_1 & 0 \\ 0 & c_2 \end{bmatrix} \,,$$
$$\mathbf{M} = mL^3 \begin{bmatrix} \frac{5}{3} + \cos q_2 & \frac{1}{3} + \frac{1}{2}\cos q_2 \\ \frac{1}{3} + \frac{1}{2}\cos q_2 & \frac{1}{3} \end{bmatrix} \,. \tag{15}$$

Solution of the linearized model

For simplicity the case where the two springs are identical is considered: $k_1 = k_2 \equiv k$ and $c_1 = c_2 \equiv c$. In the linearization, a natural configuration of interest is the straight upright trivial state of the system, $\mathbf{q}_e = 0$. The stiffness, damping and mass matrices are

$$\mathbf{K} = k \begin{bmatrix} 1 & 0 \\ 0 & 1 \end{bmatrix} + PL \begin{bmatrix} 0 & 1 \\ 0 & 0 \end{bmatrix} \,, \quad \mathbf{C} = c \begin{bmatrix} 1 & 0 \\ 0 & 1 \end{bmatrix} \,, \quad \mathbf{M} = \frac{1}{6} mL^3 \begin{bmatrix} 16 & 5 \\ 5 & 2 \end{bmatrix} \,. \tag{16}$$

For comparison, the stiffness matrix for the conservative dead-weight case with P_{cons} is

$$\mathbf{K}_{\text{cons}} = \begin{bmatrix} k_1 & 0 \\ 0 & k_2 \end{bmatrix} - P_{\text{cons}} L \begin{bmatrix} \cos q_1 + \cos(q_1 + q_2) & \cos(q_1 + q_2) \\ \cos(q_1 + q_2) & \cos(q_1 + q_2) \end{bmatrix} \,,$$

and on the trivial state $\mathbf{q}_e = 0$,

$$\mathbf{K}_{\text{cons}} = k \begin{bmatrix} 1 & 0 \\ 0 & 1 \end{bmatrix} - P_{\text{cons}} L \begin{bmatrix} 2 & 1 \\ 1 & 1 \end{bmatrix} \,.$$

Let us divide both sides of equation (13) by mL^3, and define the dimensionless quantities

$$t' \equiv \frac{t}{\tau} \,, \quad \beta \equiv \frac{c\tau}{mL^3} \,, \quad \gamma \equiv \frac{k\tau^2}{mL^3} \,, \quad \lambda \equiv \frac{PL}{k} \,. \tag{17}$$

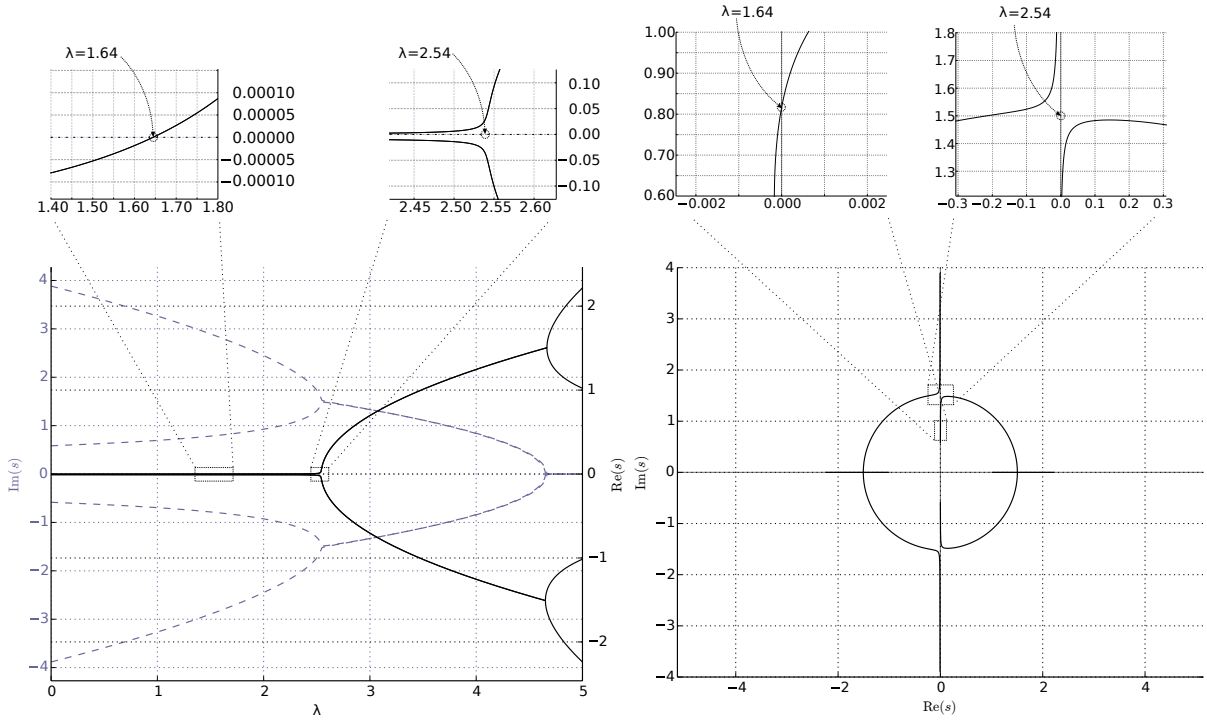

Figure 2. Solutions of the characteristic polynomial (21) for $\gamma = 1$, $\beta = 10^{-3}$. In the large left subfigure, the solid line represents $\mathrm{Re}(s)$ and the dashed line $\mathrm{Im}(s)$. The trivial equilibrium point $(q_1, q_2) = (0, 0)$ loses stability at $\lambda^{**} \approx 1.64$ in a dynamic mode (a.k.a. flutter, $\mathrm{Im}\, s \neq 0$). The bifurcation point of the undamped case, at $\lambda^{*} \approx 2.54$, is no longer a bifurcation point.

Here t' is the dimensionless time coordinate, and τ is a characteristic time (an arbitrary scaling factor). Because we are dealing with moments, in the SI system we have $[k] = \mathrm{N\,m/rad} = \mathrm{N\,m}$ and $[c] = \mathrm{N\,m\,s}$. Note also that $[m] = \mathrm{kg/m}$, the linear density of the rod material, and observe that in (13), each $\partial/\partial t$ produces a factor of $1/\tau$ when the equation is re-expressed using the dimensionless time t' (via the chain rule). The following forms are obtained for the dimensionless stiffness, damping and mass matrices:

$$\widetilde{\mathbf{K}} = \gamma \left(\begin{bmatrix} 1 & 0 \\ 0 & 1 \end{bmatrix} + \lambda \begin{bmatrix} 0 & 1 \\ 0 & 0 \end{bmatrix} \right) , \quad \widetilde{\mathbf{C}} = \beta \begin{bmatrix} 1 & 0 \\ 0 & 1 \end{bmatrix} , \quad \widetilde{\mathbf{M}} = \frac{1}{6} \begin{bmatrix} 16 & 5 \\ 5 & 2 \end{bmatrix} . \tag{18}$$

The system has three remaining parameters: β is a damping/mass ratio, γ is a stiffness/mass ratio, and λ is the loading strength relative to the reference load k/L. Thus, essentially λ may vary continuously (as a parameter), while β and γ play the role of material constants. We will perform a parametric analysis, fixing β and γ at some constant values, and examining the solutions of this system as a function of λ.

Equation (13) is a system of ordinary differential equations with constant coefficients. The standard technique is to apply the time-harmonic trial function to determine its harmonic vibrations. Inserting the trial function

$$\mathbf{q}^* = e^{s\,t'}\,\mathbf{y} \tag{19}$$

(where $\mathbf{y}$ is an eigenstate vector and s the dimensionless complex stability exponent) into the dimensionless representation of (13) and discarding the common factor $e^{s\,t'}$, the result is

$$\left(\widetilde{\mathbf{K}} + s\widetilde{\mathbf{C}} + s^2 \widetilde{\mathbf{M}} \right) \mathbf{y} = 0 \, , \tag{20}$$

which has nontrivial solutions $\mathbf{y} \not\equiv 0$ if and only if the determinant vanishes. Using (18) and (20), we construct the characteristic polynomial, which is of the fourth order in the stability

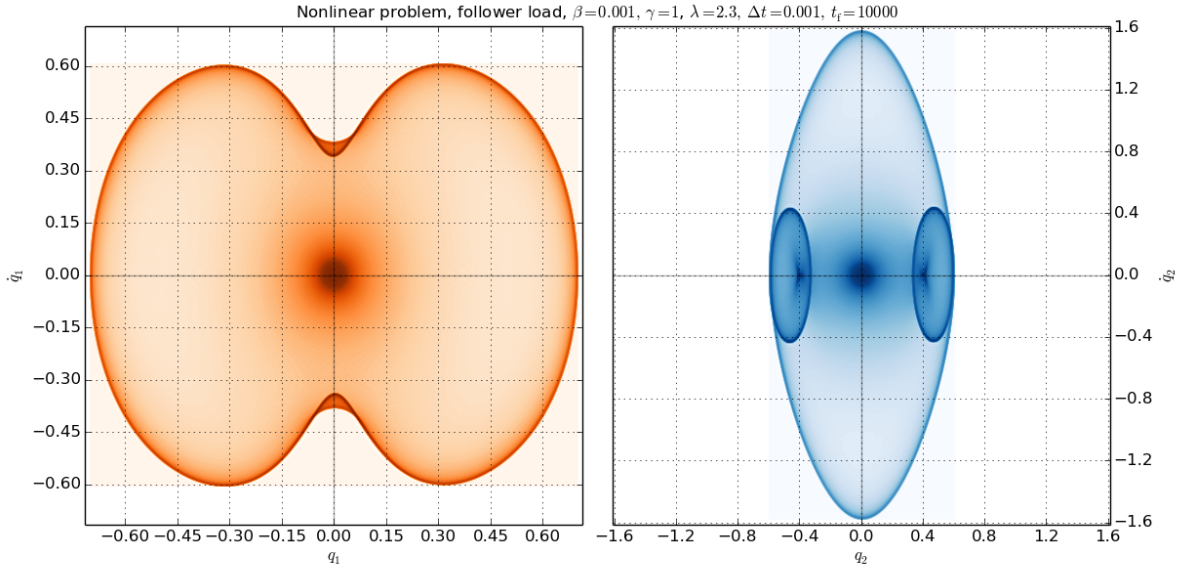

Figure 3. A solution of the non-linear system. Phase space density plots for $(q_1, \dot{q}_1)$ and $(q_2, \dot{q}_2)$ for $\gamma = 1$, $\beta = 10^{-3}$, $\lambda = 2.3$ with initial condition $(q_1, \dot{q}_1, q_2, \dot{q}_2) = (10^{-3}, 0, 10^{-3}, 0)$.

exponent s. The zeroes of this polynomial give the admissible values of the stability exponent at each point (β, γ, λ) in the parameter space. Explicitly, for the non-conservative problem it is obtained that

$$\left[\gamma + s(\beta + \frac{8}{3}s)\right]\left[\gamma + s(\beta + \frac{1}{3}s)\right] - \left[\gamma\lambda + \frac{5}{6}s^2\right]\left[\frac{5}{6}s^2\right] = 0\,. \tag{21}$$

For comparison, for the conservative (dead-weight) problem the characteristic polynomial is

$$\left[\gamma(1-2\lambda) + s(\beta + \frac{8}{3}s)\right]\left[\gamma(1-\lambda) + s(\beta + \frac{1}{3}s)\right] - \left[-\gamma\lambda + \frac{5}{6}s^2\right]\left[-\gamma\lambda + \frac{5}{6}s^2\right] = 0\,.$$

For a numerical example, let us choose $\gamma = 1$ and the range $\lambda = [0, 5]$. The solutions of the non-conservative case (21) are shown in Fig. 2. By the introduction of small damping into the model, the critical value of the load parameter has jumped down from $\lambda^* \approx 2.54$ to $\lambda^{**} \approx 1.64$; this behaviour is retained for arbitrarily small positive β. One pair of solutions crosses the imaginary axis well before the undamped bifurcation load λ^* is reached.

Solution of the non-linear model

To illustrate the behaviour of the original non-linear system, we perform direct time integration up to a prescribed end time $t'_f = 10\,000$ (with trivial time scaling, $\tau = 1\,\mathrm{s}$), choosing the load λ such that $\lambda^{**} < \lambda < \lambda^*$. By introduction of auxiliary variables for $\dot{q}_1$ and $\dot{q}_2$, the non-linear system (7) with the definitions in Eqs. (6) is reduced to the standard first-order form

$$\dot{\mathbf{w}} = f(\mathbf{w})\,, \quad \text{where } \mathbf{w} = (q_1, \dot{q}_1, q_2, \dot{q}_2)\,. \tag{22}$$

The classical implicit midpoint rule (IMR) is used to integrate the equations of motion. The integration is performed at a constant timestep, because in addition to simplicity, this leads to a property that is very useful for visualization. Consider a projection of the trajectory, where the time coordinate is projected away (discarded). The time-discretized solution forms a four-dimensional point cloud in the state space $(q_1, \dot{q}_1, q_2, \dot{q}_2)$. With a constant timestep, the local density of the point cloud is linearly proportional to the portion of total simulated time that the time-discretized system spends in that local region of the state space.

To visualize the results, the time coordinate is discarded, and the four-dimensional data is projected into two dimensions. Two physically motivated, independent projections are used; the first projection is $(q_1, \dot{q}_1)$ and the second is $(q_2, \dot{q}_2)$.

A simple kernel density estimator is applied to the resulting two-dimensional point clouds, in order to extract a discrete (raster) representation of the state space density function. Kernel density estimation is preferable over 2D histogramming, because it gives subpixel accuracy (reducing moiré artifacts), and it is not sensitive to the placement of the bin edges.

The density function has a high dynamic range, far exceeding that which is representable on a computer screen or in print. To visualize the density, a dynamic range compressor is applied before plotting. We choose the data-adaptive histogram remapping method of Larson, Rushmeier and Piatko [7], which preserves visual contrast. The resulting colour scale is neither linear nor logarithmic; instead, the colours are allocated in a data-adaptive manner in order to reveal as much structure in the data as possible. For details, see [8].

See Fig. 3 for the results. The parameters are $\beta = 10^{-3}$, $\gamma = 1$ and $\lambda = 2.3$. The shade is a monotonic function of the state space density, with darker shades indicating higher densities. The solution starts at the initial point $(q_1, \dot{q}_1, q_2, \dot{q}_2) = (10^{-3}, 0, 10^{-3}, 0)$, spirals out at first slowly (dark region near origin), and accelerates outward (shade becomes lighter). Then the non-linearity starts to have a visible effect, slowing the outward motion (shade becomes darker again) and deforming the trajectory into a more complicated shape. Eventually, the system settles onto a limit cycle (dark outer border; in the right subfigure, including the outline and the small ellipses) far away from the initial point. In this cycle, while the ranges of angles for both springs are approximately the same, the second rod has a higher maximum angular velocity.

The non-linear simulation illustrates the global meaning of the local instability of the static equilibrium at the origin for $\lambda = 2.3$, indicated by the linear analysis in Fig. 2. As is common for non-linear systems, the exponential growth of the solution norm eventually stops, and the system settles onto an attractor, which in this particular case is a limit cycle. Studying the non-linear problem parametrically, also strange attractors can be found for higher values of λ. No further static equilibria exist; by requiring $\ddot{\mathbf{q}} = \dot{\mathbf{q}} = 0$ in (7) and solving for $\mathbf{q}$, it is seen that the origin is the only static equilibrium point for the non-linear system with the follower load.

References

[1] H. Ziegler. Die Stabilitätskriterien der Elastomechanik. *Ingenieur Archiv*, **20**, 1952, 49–56.

[2] V.V. Bolotin. *Nonconservative Problems of the Theory of Elastic Stability.* Pergamon Press, 1963.

[3] V.V. Bolotin. Dynamic stability of structures. In *Nonlinear Stability of Structures*, Series CISM No 342. A.N. Kounadis and W.B. Krätzig (Eds.) Springer, 1995, 3–72.

[4] Y. Sugiyama and M.A. Langthjem. Physical mechanisms of the destabilizing effect of damping in continuous non-conservative dissipative systems. *International Journal of Non-linear Mechanics*, **42**, 2006, No 1, 132–145.

[5] Q.S. Nguyen. *Bifurcation and Stability of Dissipative Systems*, Springer-Verlag, 1993, CISM courses and lectures no. 327.

[6] Q.S. Nguyen. *Stability and Nonlinear Solid Mechanics.* John Wiley & Sons, 2000.

[7] G. Larson, H. Rushmeier and C. Piatko. Visibility Matching Tone Reproduction Operator for High Dynamic Range Scenes. *IEEE Transactions on Visualization and Computer Graphics*, **3**, 1997, 291–306.

[8] J. Jeronen. Visual contrast preserving representation of high dynamic range mathematical functions. In *Numerical methods for differential equations, optimization, and technological problems. Dedicated to Professor P. Neittaanmäki on his 60th Birthday.*, Series Computational Methods in Applied Sciences No 27. S. Repin, T. Tiihonen and T. Tuovinen (Eds.) Springer, 2013, 409–429.